ACS APPLIED MATERIALS & INTERFACES

Research Article

www.acsami.org

Tuning Open-Circuit Voltage in Organic Solar Cells with Molecular Orientation

Brent Kitchen,[†] Omar Awartani,[†] R. Joseph Kline,[‡] Terry McAfee,[§] Harald Ade,[§] and Brendan T. O'Connor*[,†]

[†]Department of Mechanical, Aerospace Engineering, North Carolina State University, 911 Oval Drive, Raleigh, North Carolina 27695, United States

[‡]Material Measurement Laboratory, National Institute of Standards and Technology, 100 Bureau Drive, Gaithersburg, Maryland 20899, United States

[§]Department of Physics, North Carolina State University, 2401 Stinson Drive, Raleigh, North Carolina 27695, United States

Supporting Information

ABSTRACT: The role of molecular orientation of a polar conjugated polymer in polymer–fullerene organic photovoltaic (OPV) cells is investigated. A planar heterojunction (PHJ) OPV cell composed of poly(3-hexylthiophene) (P3HT) and [6,6]-phenyl C61-butyric acid methyl ester (PCBM) is used as a model system to isolate the effect of the interfacial orientation on the photovoltaic properties. The molecular orientation of the aggregate P3HT relative to the PCBM layer is varied from highly edge-on (conjugated ring plane perpendicular to the interface plane) to appreciably face-on (ring plane parallel to the interface). It is found that as the P3HT stacking becomes more face-on there is a positive correlation to the OPV open-circuit voltage (V_{OC}), attributed to a shift in the highest occupied molecular orbital (HOMO) energy level of P3HT. In addition, the PHJ OPV cell with a broad P3HT stacking orientation distribution has a V_{OC} comparable to an archetypal bulk heterojunction (BHJ) device. These results suggest that, in the BHJ OPV cell, the hole energy level in the charge transfer state is defined in part by the orientation distribution of the P3HT at the interface with PCBM. Finally, the photoresponses of the devices are also shown to have a dependence on P3HT stacking orientation.

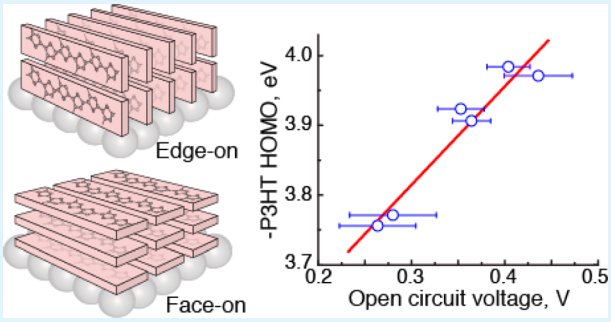

KEYWORDS: *solar cells, organic electronics, open-circuit voltage, molecular orientation*

1. INTRODUCTION

In organic solar cells the photoactive layer typically consists of an electron donor and an electron acceptor material with offsets in their highest occupied molecular orbital (HOMO) and lowest unoccupied molecular orbital (LUMO) energy levels. Given the low dielectric constant and weak intermolecular coupling character of organic semiconductors, light absorption results in the formation of Coulombically bound electron–hole pairs, or excitons, and the heterojunction provides a driving force to efficiently dissociate the excitons into free charge carriers. The difference in the HOMO of the donor and LUMO of the acceptor is also directly related to the open-circuit voltage (V_{OC}) of the solar cell.[1−4] Given the critical nature of the heterojunction on organic photovoltaic (OPV) device performance, there has been a significant amount of research considering energy level alignment at the interface, charge transfer states, and dipole interactions.[2−12] Recently, the role of molecular orientation at the heterojunction interface has been investigated in a number of OPV systems,[5,6,9,13] where the relative molecular orientation has been shown to significantly influence device performance including charge transfer dissociation and recombination rates.[5,6] The orientation of polar organic molecules is also expected to alter the molecular energy levels of frontier orbitals, which then vary the output voltage of the solar cell.[12,14] However, there has not been a detailed experimental analysis on the variation in V_{OC} with polar molecule orientation in OPV devices, and in particular in polymer:fullerene systems.[6,11]

Here, we consider the effect the out-of-plane stacking orientation of the quadrupolar donor polymer poly(3-hexylthiophene) (P3HT) relative to the acceptor ([6,6]-phenyl C61-butyric acid methyl ester) (PCBM) on OPV V_{OC}. Given the widespread use of P3HT, details of the energy conversion process in P3HT/PCBM solar cells have been considered at length.[1,15,16] However, probing the interface in polymer–fullerene systems such as P3HT/PCBM is difficult due to the typical approach of solution processing with common solvents resulting in the formation of a bulk heterojunction (BHJ).[16] In

Received: December 15, 2014
Accepted: June 1, 2015
Published: June 1, 2015

DOI: 10.1021/am508855s
ACS Appl. Mater. Interfaces 2015, 7, 13208−13216

this study, we form planar heterojunction (PHJ) OPV cells with sharp interfaces to simplify the system under consideration. The PHJ OPV cells were fabricated using a transfer printing approach that has previously been shown to form a sharp interface between the printed layers.[17−20] Intermixing has been found in transfer printed films under low thermal annealing temperatures.[17,21] Here, we are careful to avoid any solvent or thermal annealing that would cause undesired mixing following previously described methods.[19,20] The transfer printing approach allows each layer of the OPV cell to be individually processed on a separate substrate to precisely control film morphology. To this end, the processing conditions of the P3HT layer were varied to alter the out-of-plane molecular stacking orientation. Key differences in film processing were the choice of solvent, spin-cast speed, and the application of large biaxial strains.[22,23] Briefly, the biaxial strain process consists of consecutively straining the P3HT films by 100% in transverse directions resulting in films with the greatest face-on stacking characteristics as experimentally characterized below, and in a recent report.[24] Altogether, there are six unique processing conditions for the P3HT films, with processing details given in Table 1. The processing conditions of the PCBM layer were held constant in all cases to isolate the effects of the P3HT morphology. The P3HT film thicknesses were kept between 36 and 45 nm, and the PCBM film thickness was held constant at ≈38 nm. The thicknesses of the P3HT and PCBM layers were selected on the basis of optimizing the PHJ OPV power conversion efficiency, and are similar to previous reports on P3HT/PCBM PHJ solar cells.[25]

Table 1. List of Processing Conditions for the P3HT Films Applied to the PHJ Solar Cells and Processing Conditions for the P3HT:PCBM BHJ Solar Cell

film name[a]	solvent	solution conc (mg/mL)	spin speed (rpm)	thickness (nm)	RMS roughness (nm)
CF-S	CF	3	500	42	0.75
CF-F	CF	6	3000	36	0.58
CF-X	CF	7	750	41	1.51
DCB-S	DCB	6	625	42	2.8
DCB-F	DCB	12	3000	37	1.29
DCB-X	DCB	12	850	45	6.5
BHJ	DCB	30	600	220	

[a]The solvent is either chloroform (CF) or 1,2-dichlorobenzene (DCB). The film is designated by S for slow spin-cast speed, F for fast spin-cast speed, or X for biaxially strained. The BHJ solution was cast from a 1:1 P3HT:PCBM ratio by mass.

2. RESULTS AND DISCUSSION

2.1. Bilayer Morphology Characterization. The packing characteristic of the crystalline P3HT was measured with grazing incidence X-ray diffraction (GIXD), with 2-D image plate data shown in Figure 1. It can be seen that there is a range of diffracting characteristics of the P3HT films depending on processing conditions. The slow cast film from the solvent 1,2-dichlorobenzene (DCB) shows the highest degree of edge-on stacking (conjugated ring plane perpendicular to the interface plane) with alkyl-stacking (h00) peaks out-of-plane and a $\pi-\pi$ stacking (020) peak observed in-plane. The biaxially strained films cast from chloroform (CF) have the highest degree of face-on stacking (conjugated ring plane parallel to the interface plane) with the (020) peak observed primarily out-of-plane. It

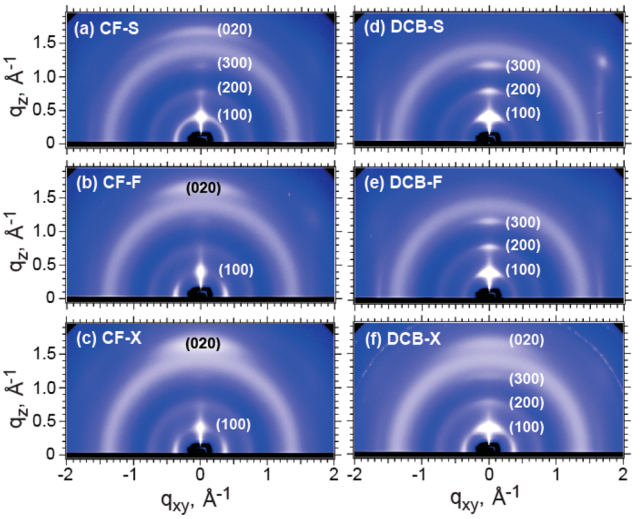

Figure 1. (a−f) Grazing incidence X-ray diffraction of all PHJ films in this study. The P3HT films are cast from chloroform (CF) and dichlorobenzene (DCB). Slow (S), fast (F), and strain (X) refer to P3HT processing conditions described in Table 1. For the biaxially strained films, the measurement is made with the beam parallel to the second strain direction.

is important to note that it has previously been demonstrated that the crystalline P3HT in the biaxially strained films show very weak preferential alignment of the backbone along the strain directions,[23] and are considered isotropically distributed in the plane of the film in this study. The orientation distribution of the diffracting P3HT is approximated by constructing a pole figure from the image plate data based on the (100) scattering peak, provided in Figure 2. From the pole

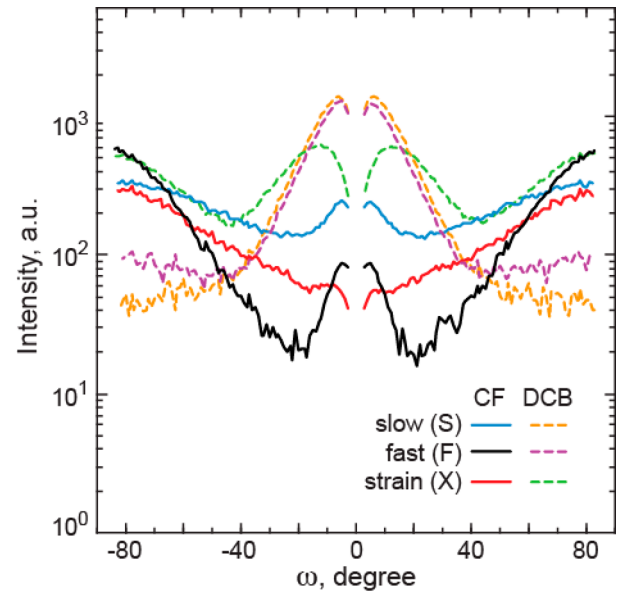

Figure 2. Pole figure of the P3HT (100) stacking peak obtained from the GIXD data to illustrate the P3HT film texture. The data is normalized by the sum of the intensity for each film, and then corrected by sin(ω). For the biaxially strained films, the pole figure is given here for the X-ray beam parallel to the second strain direction. The pole figure for the biaxially strained film with the X-ray beam parallel to the first strain direction is given in Supporting Information Figure S3, and both pole figures are found to be similar.

DOI: 10.1021/am508855s
ACS Appl. Mater. Interfaces 2015, 7, 13208−13216

figure, the stacking character of the P3HT is shown to vary from highly edge-on to films with significant amounts of face-on stacking. Note that since the GIXD data is taken at fixed incident angle, the pole figure for the (100) can only measure ω angles greater than 1.7° ($2\theta_{Bragg}/2 - \theta_{incident}$). Crystals oriented at smaller angles are not measured. For these films, the unmeasured crystals are negligible because no significant highly oriented scattering is observed for the in-plane π-stacking and the geometric $\sin(\omega)$ correction means that any such crystals make an insignificant contribution to the total crystal concentration. This is consistent with the 2-D images, and thus, the (100) diffraction peak is considered representative of the orientation distribution of the crystalline P3HT in the film. Furthermore, while the GIXD probes the bulk of the film, it has been shown to track well with the average surface orientation in spun cast[21] and biaxially strained[24] films as measured using near-edge X-ray absorption fine structure (NEXAFS) spectroscopy. Therefore, we consider the near surface P3HT crystal orientation to be consistent with the orientation of the diffracting P3HT measured by GIXD.

To compare differences in P3HT local aggregate order for the various processing conditions, the films were measured using UV−vis absorption spectroscopy, with the normalized absorbance given in Figure 3. It is observed that films cast from

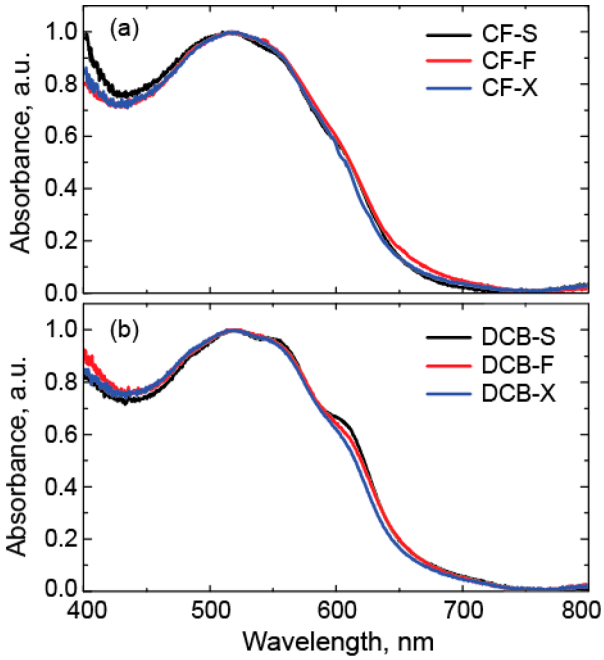

Figure 3. Absorbance of the bilayer P3HT/PCBM films for (a) P3HT films cast from chloroform (CF) and (b) films cast from dichlorobenzene (DCB). The measurements are for P3HT films fabricated with a slow spin-cast speed (S), fast spin-cast speed (F), and biaxial strain (X) as detailed in Table 1.

the same solvent have similar absorbance spectra, with relatively little difference between spin-cast speed and the application of strain. However, the films cast from DCB have slightly sharper absorbance features at 505 and 605 nm than films cast from CF. These absorbance features arise from vibronic coupling of parallel-aligned, cofacially packed conjugated chains that can be described by a weakly interacting H-aggregate model.[15,26,27] This model can be used to estimate the local aggregate order (described by the Gaussian line width, σ), the width of interacting aggregates (described by the exciton bandwidth, W), and the percentage of aggregate P3HT in the film.[27] Applying this model to the absorbance data in Figure 3, σ and percent P3HT aggregate are found to be relatively constant with a variation from 77 to 90 meV and 45% to 48%, respectively. This assumes all films have a similar polymer long-axis orientation distribution with respect to the substrate. The largest change in the H-aggregate model fit is the exciton bandwidth, which is found to decrease when going from films cast from DCB solvent (average W = 103 meV) to films cast from CF solvent (average W = 83 eV). This change corresponds to a change in the aggregate width along the backbone direction from approximately 43 to 35 thiophene units.[15,28] Additional details of the model and fitting results are provided in the Supporting Information. The absolute absorbance of the films is also given in Supporting Information Figure S2, where all films are found to have a similar magnitude, as expected given the similar film thickness. The similar absorbance indicates that light absorption in the P3HT layer will be similar when applied in an OPV device. While crystallinity and percent aggregate are not the same, this measurement suggests similar levels of local order between films.

Finally, the surface roughness of the P3HT layer may influence device performance and requires characterization. The P3HT film topography, for the surface that is in intimate contact with the PCBM layer in the OPV cell, was measured with atomic force microscopy (AFM) prior to device fabrication with characteristic images given in Figure 4. The RMS roughness of the film surface is given in Table 1 showing that the fast spun cast films had the lowest RMS roughness followed by slow spun films and then the biaxially strained films. During device processing, the PCBM layer is printed onto this P3HT surface without significant applied pressure, and the P3HT/PCBM interface roughness is expected to be similar to the surface roughness of the P3HT layer prior to printing.

In summary, the largest change in morphology between processing conditions is the out-of-plane P3HT stacking orientation, which varies widely from edge-on to face-on depending on processing conditions. There is also a variation in surface roughness as measured by atomic force microscopy, where the higher spin-cast speed results in smoother films and the biaxial strain process increases surface roughness. The relatively weak vibronic character observed in the absorbance spectrum and the similar estimated percent aggregate (45−48%) suggest all P3HT films have similar levels of local order. From the absorbance, the estimated variation in the number of interacting thiophene units in the aggregate P3HT is not expected to contribute to appreciable differences in electronic structure. Lastly, the similar film quality between spun cast and biaxially strained films is also highlighted by previous work that showed that these films have similar in-plane field effect mobility when applied in a field effect transistor configuration.[24]

2.2. Photovoltaic Device Characteristics. To determine the role of P3HT morphology on device performance, PHJ OPV cells consisting of the six unique P3HT processing conditions were fabricated and characterized. The current density−voltage (J−V) characteristics of the PHJ OPV cells under 1-sun illumination are given in Figure 5 with key performance metrics provided in Table 2. The efficiency of these planar devices is considerably lower than that of their BHJ counterpart as a result of the much smaller interfacial area

DOI: 10.1021/am508855s
ACS Appl. Mater. Interfaces 2015, 7, 13208−13216

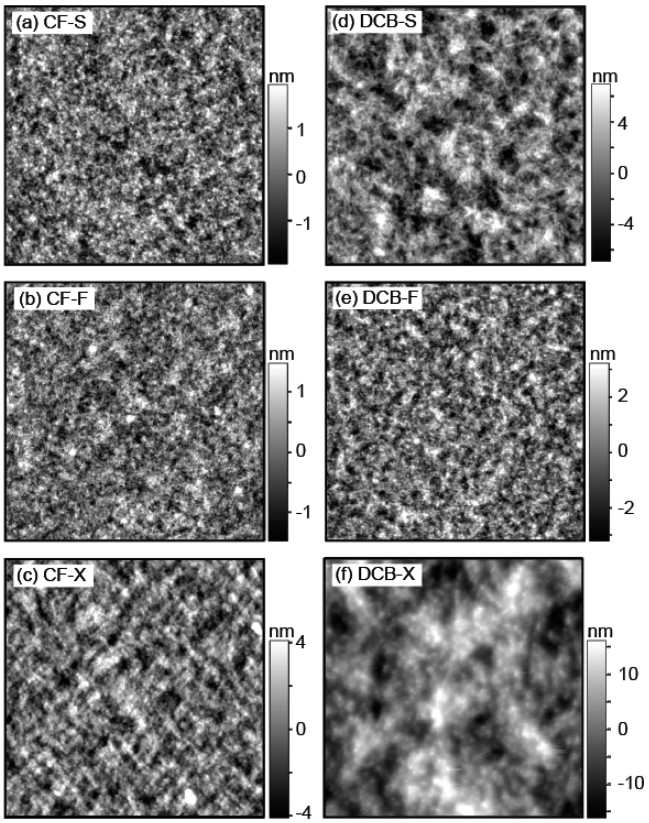

Figure 4. Characteristic AFM images for the different P3HT processing conditions outlined in Table 1 including (a) CF-X, (b) CF-F, (c) CF-X, (d) DCB-S, (e) DCB-F, and (f) DCB-X. The area of each image is 2.5 μm × 2.5 μm. The RMS roughness calculated from these images is given in Table 1.

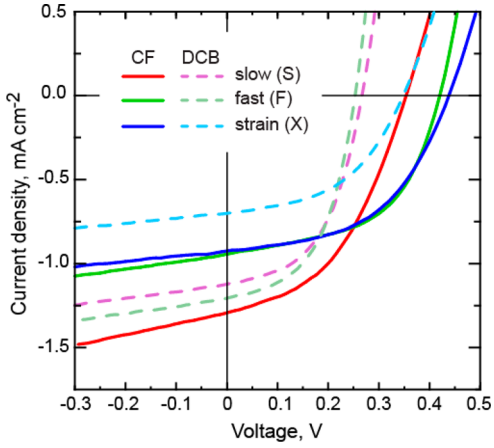

Figure 5. Current density−voltage relationship for characteristic PHJ OPV cells under 1-sun illumination conditions (100 mW cm^{-2}). The P3HT films are cast from chloroform (CF) and dichlorobenzene (DCB), with additional processing details described in Table 1.

between the P3HT and PCBM.[25,29] When these PHJ cells are thermally annealed at 110 °C, the P3HT and PCBM layers intermix resulting in a thin BHJ device with power conversion efficiencies of approximately 2.5%. The key difference observed in the PHJ device performance in this study is the variation in V_{OC} and short circuit current density (J_{SC}). As the P3HT stacking in the OPV cell becomes more face-on, there is a corresponding increase in V_{OC}. The reverse trend is observed for J_{SC} for each set of films with common starting solvent.

To gain insight into the OPV cell performance, the dark current density characteristics for the devices plotted in Figure 5 are fit to the generalized Shockley equation,[8]

$$J = \frac{R_P}{R_S + R_P}\left\{J_0\left[\exp\left(\frac{e(V - JR_S)}{nKT}\right) - 1\right] + \frac{V}{R_P}\right\} \quad (1)$$

where R_P is the shunt resistance, R_S is the series resistance, J_0 is the dark saturation current density, e is the electron charge, K is the Boltzmann constant, T is temperature, and V is voltage. From this model, R_S, R_P, and J_0 are extracted, with best-fit values for each device provided in Table 2, and fits to the dark current data plotted in Supporting Information Figure S4. The ideality factor (n) was also fit using eq 1 and found to be approximately 1.7 for all devices. We find that R_S and R_P vary between devices; however, the differences are not expected to contribute significantly to device performance variation as discussed below and in more detail in the Supporting Information.[6,8] Contrasting the relatively similar values for n, R_P, and R_S, J_0 is found to vary significantly between devices, decreasing as the P3HT stacking becomes more face-on. This variation in J_0 can be correlated to V_{OC}, where under open-circuit conditions eq 1 can be simplified to

$$V_{OC} = \frac{nKT}{e}\ln\left(\frac{J_{SC}}{J_0}\right) \quad (2)$$

with the approximation that R_P is large and R_S is small. The correlation between V_{OC} and J_0 for the devices is given in Figure 6 along with the theoretical variation of V_{OC} with change in J_0 based on eq 2 for J_{SC} = 1 mA cm^{-2} and n = 1.7. The predicted V_{OC} is shown to be in good agreement with the experimental values, highlighting the minimal effect that the variations in short circuit current and resistances have on the measured V_{OC}. Furthermore, J_0 can also be given by[4,8]

$$J_0 = J_{00}\exp\left(\frac{-\Delta E_{HL}}{2n'KT}\right) \quad (3)$$

where J_{00} is the current prefactor, T is temperature, and ΔE_{HL} is the difference between the HOMO of the donor (P3HT) and LUMO of the acceptor (PCBM). A modified ideality factor is given here as n', which relates the activation energy in the Arrhenius behavior of J_0 to ΔE_{HL}. This factor can be attributed to the thermal excitation of free carriers at the heterojunction, as well as influences from interface states.[4,30,31] Combining eqs 2 and 3 results in

$$eV_{OC} = \frac{n}{n'}\Delta E_{HL} + nKT\ln\left(\frac{J_{SC}}{J_{00}}\right) \quad (4)$$

which provides a linear relationship between V_{OC} and ΔE_{HL} with a modification based on the saturation current prefactor. The factors in this equation that contribute most significantly to the change in V_{OC} are discussed below in further detail. When considering the device V_{OC}, it is important to note that the choice of electrodes can impact the V_{OC} of OPV cells.[32] However, Fermi level pinning at the interface between P3HT and the adjacent hole transport layer pol(3,4-ethylenedioxythiophene):poly(styrenesulfonate) (PEDOT:PSS) is expected.[2] This should result in the HOMO of

DOI: 10.1021/am508855s
ACS Appl. Mater. Interfaces 2015, 7, 13208−13216

Table 2. Performance of the Solar Cells under 1-sun Illumination

film name	J_{SC}[a] (mA/cm^2)	V_{OC}[a] (V)	fill factor[a]	efficiency[a] (%)	R_P[b] (MΩ cm^2)	R_S[b] (Ω cm^2)	J_0[b] (μA/cm^2)
CF-S	1.24 ± 0.11	0.35 ± 0.03	0.50 ± 0.05	0.22 ± 0.03	0.10	5	0.25
CF-F	0.82 ± 0.17	0.40 ± 0.02	0.53 ± 0.01	0.18 ± 0.05	1.00	40	0.03
CF-X	0.87 ± 0.16	0.44 ± 0.03	0.50 ± 0.03	0.19 ± 0.03	0.95	60	0.05
DCB-S	1.11 ± 0.08	0.26 ± 0.04	0.49 ± 0.02	0.12 ± 0.02	0.17	10	2.00
DCB-F	1.15 ± 0.15	0.28 ± 0.05	0.50 ± 0.01	0.16 ± 0.02	0.15	50	3.00
DCB-X	0.68 ± 0.04	0.36 ± 0.02	0.48 ± 0.02	0.12 ± 0.01	2.00	50	0.08

[a]Average values with standard deviation given. [b]Represents data from characteristic devices.

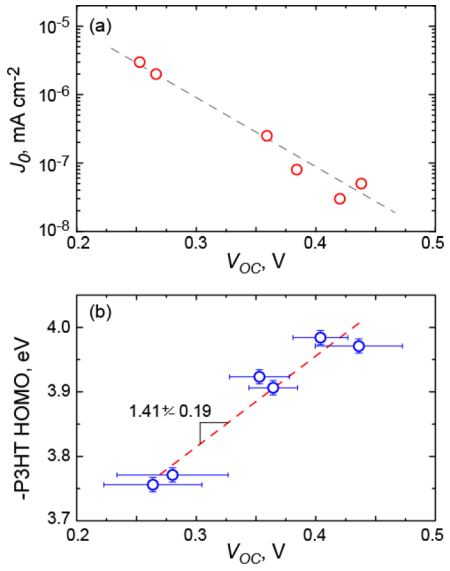

Figure 6. (a) Reverse saturation current (J_0) determined by fitting an equivalent circuit model to the dark current−voltage characteristics of the OPV cells compared to the open-circuit voltage (V_{OC}) under illumination. The symbols are for experimentally determined V_{OC}, and the dashed line is the V_{OC} dependence based on eq 2. (b) A comparison between the P3HT HOMO energy estimated from the XRD pole figure and DFT, and the OPV V_{OC}. The dashed line is a linear fit to the data resulting in a slope of 1.41 ± 0.19. The data is given as the negative of the P3HT HOMO energy level to represent a positive increase in ΔE_{HL}.

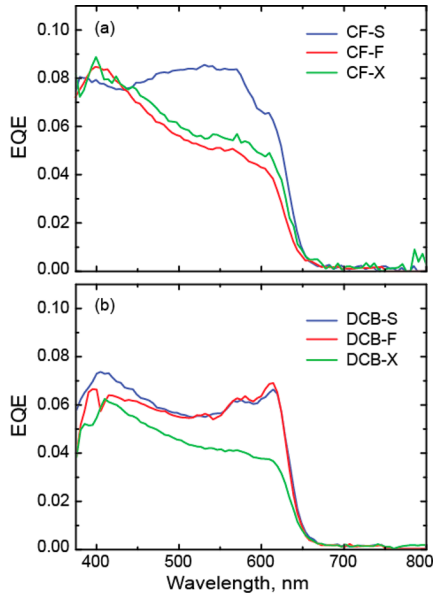

Figure 7. External quantum efficiency (EQE) for the PHJ OPV cells for (a) P3HT films cast from chloroform (CF) and (b) P3HT films cast from dichlorobezene (DCB). The processing conditions of the P3HT include slow spin-cast speed (S), fast spin-cast speed (F), and biaxial strain (X) as detailed in Table 1.

the P3HT film dictating the output voltage rather than the PEDOT:PSS layer.

To consider the origin of the differences observed in J_{SC}, the external quantum efficiency (EQE) was measured for each device, given in Figure 7. The predicted J_{SC} obtained by integrating the product of the EQE with AM1.5G photon flux generally shows good agreement with the J_{SC} measured with the solar simulator with results given in Supporting Information Table S1. It is observed that the differences in EQE are greatest over the portion of the spectrum dominated by aggregate P3HT absorption suggesting that the origin of the variation in photocurrent is related to the molecular orientation of the P3HT, discussed below in more detail. The variation in out-of-plane P3HT stacking characteristics may also influence device performance by altering the charge collection efficiency due to changes in out-of-plane hole mobility.[33] To determine if there is a significant difference in hole mobility, single carrier diodes were fabricated for each P3HT processing condition. From the $J-V$ characteristics, the hole mobility was found to be $60 \times 10^{-6} \pm 40 \times 10^{-6}$ cm^2 V^{-1} s^{-1} with no significant difference found between devices, particularly for films with a common starting solvent. The uncertainty is based on the pooled standard deviation of all devices. Therefore, the change in out-of-plane P3HT stacking for the films under consideration does not appear to have a significant influence on out-of-plane hole mobility.

2.3. Discussion. The variation in open-circuit voltage with molecular orientation has been previously considered theoretically by Heimel et. al,[14] where density functional theory (DFT) models suggested that the ionization energy and the electron affinity of P3HT can change by up to 0.5 eV between perfectly face-on and edge-on configurations with respect to vacuum.[14] This is attributed to an intrinsic surface dipole in P3HT along the conjugated backbone. From the DFT model, the change in ionization energy (IE) with stacking orientation was analytically described by[14]

$$\mathrm{IE}(\theta) = \mathrm{IE}_0 + \frac{e}{\varepsilon_0}\frac{\mu_\pi \cos(\theta)}{c[b + (a-b)\cos(\theta)]} \quad (5)$$

where IE_0 is the ionization energy in the absence of a surface dipole taken here as 3.42 eV, e is electron charge, ε_0 is the free space permittivity, μ_π is the intrinsic surface dipole taken as 7.37×10^{-30} Cm, and θ is the conjugated ring plane angle with respect to the plane of the film. The characteristic lengths a, b, and c are the interlamellar distance (1.73 nm), π-stacking distance (0.39 nm), and monomer extension (0.78 nm), respectively.[14] This analytical expression suggests that,

DOI: 10.1021/am508855s
ACS Appl. Mater. Interfaces 2015, 7, 13208−13216

assuming vacuum level alignment, an edge-on orientation of the P3HT relative to the heterojunction leads to a higher-lying HOMO level, and thus a smaller difference between the HOMO of the donor (P3HT) and LUMO of the acceptor (PCBM) resulting in a smaller OPV V_{OC}.

The IE of the P3HT films under study is estimated by taking a density weighted average of IE(θ) from eq 5 for each P3HT crystal stacking orientation, where the orientation distribution of P3HT is taken from the pole figure data in Figure 2. To get an accurate measure of the relative concentration of crystallites with a given orientation, a sin(ω) correction was applied to the pole figure.[34] The estimated IE of each film is compared to the film OPV V_{OC} in Figure 6b showing a linear relationship with a slope of 1.41 ± 0.19. Comparing this correlation to eq 4, the linear relationship between V_{OC} and ΔE_{HL} suggests that the change in V_{OC} is due to the change in the P3HT HOMO level consistent with the DFT model. While the absolute charge transfer state HOMO energy level may differ from the IE of the neat polymer with respect to vacuum as predicted by DFT, the orientation dependence is expected to follow a similar trend. The change in J_{00} may also influence V_{OC};[35] however, the linear relationship in Figure 6b suggests that the logarithmic term that includes J_{00} is not a large contributing factor. Additionally, it has been shown that J_{00} can be related to the electronic coupling at the heterojunction,[35,36] and that this may impact V_{OC}. However, it has been shown that, for a range of OPV material systems, J_{00} does not significantly influence the open-circuit voltage of the device.[35,36] This includes OPV devices with P3HT and a range of fullerene derivatives.[35]

It is worth noting that the slope of 1.41 found in Figure 6b does not correspond to the slope predicted using eq 4 of n/n'. Here, n under illumination is approximately 1.4, found from eq 2 and the slope of V_{OC} with J_{SC} given in Figure 8. In a wide range of heterojunctions n' is commonly found to be close to 2.[4,30,31] This results in a slope closer to 0.7. One aspect of the P3HT film not accounted for is the molecular stacking orientation of the amorphous fraction of the film. The percentage aggregate of the P3HT films was estimated above to be between 45% and 48% by absorption analysis. Although percent aggregate and percent crystallinity are not the same, the aggregates are likely to have a similar packing distribution as the diffracted material. The percent aggregate estimate suggests that there is about 50% amorphous material that might not be accounted for by the GIXD pole figure measurement. Assuming the amorphous, nonscattering polymer does not have a strong out-of-plane stacking preference, it will reduce the predicted change in open-circuit voltage resulting in a slope closer to the theoretical n/n'. However, additional analysis beyond the scope of this work is required to place physical significance to the slope in Figure 6b.

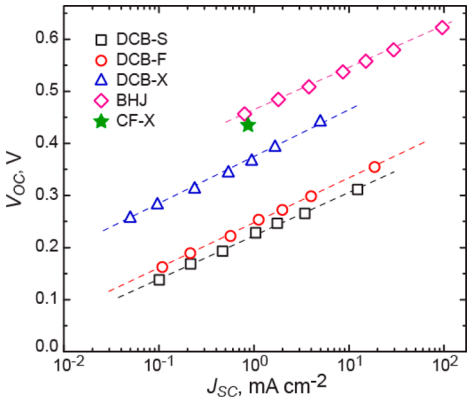

Figure 8. Open-circuit voltage (V_{OC}) vs short circuit current (J_{SC}) of PHJ and BHJ OPV cells all cast from dichlorobenzene (DCB) under variable light intensity. The natural log slope of the data is found to be between 0.034 and 0.038 for all devices. The average V_{OC} of the PHJ OPV cells with biaxially strained P3HT films cast from chloroform (CF-X) under 1-sun illumination conditions is also plotted for comparison.

It is somewhat surprising that averaging the IE(θ) of the P3HT with various orientations correlates well with the variation in V_{OC}. However, this result is similar to that found in ternary organic solar cells, which are devices made up of a donor or acceptor component that consists of two complementary materials.[37] In these systems, there is a continuous variation in the device V_{OC} with the ratio of the two-component pair with limits in V_{OC} defined by the ratio limit of 0 and 1 of the pair. Recently, the origin of this continuous variation in V_{OC} has been attributed to the delocalized nature of the hole (electron) in the charge transfer state that reflects the average composition of the donor (acceptor) pair.[37] Similarly, given the semicrystalline nature of P3HT, the hole wave function is expected to be significantly delocalized, and the HOMO energy level of the charge transfer state should be a compositional average of the local orientation distribution of the P3HT.

A comparison of the V_{OC} of the PHJ OPV cells cast from DCB to the more common BHJ OPV cell is given in Figure 8. In organic solar cells V_{OC} is dependent on current density,[38] and a comparison between V_{OC} should be made at a common J_{SC}. To compare devices at common J_{SC} values, the V_{OC} and J_{SC} are measured over a range of illumination intensities. As shown in Figure 8, The V_{OC} of the more face-on biaxially strained P3HT OPV cell (DCB-X) approaches the BHJ device. While the V_{OC} is lower in the PHJ cell, the biaxially strained film cast from DCB still has a large edge-on stacking P3HT component. The performance of the film with the highest face-on stacking character, biaxially strained P3HT (CF-X), is also given in Figure 8 for 1-sun illumination conditions. In this comparison, the CF-X OPV cell has a V_{OC} comparable to that of the BHJ device. This suggests that the local energetic environment of the P3HT at the heterojunction in a BHJ device is similar to that of the CF-X PHJ cell. In a BHJ OPV cell, it is unlikely that there is a strong stacking preference of P3HT with respect to PCBM.[16] Under these conditions the HOMO energy level of the charge transfer state is consistent with the broad orientation distribution of the biaxially strained P3HT film cast from CF.

The variation in short circuit current may be attributed to a number of factors including differences in interfacial roughness, exciton diffusion lengths, active layer thickness, or charge transfer state coupling and dissociation efficiency. From Figure 7, the variation in photoresponse is dominated by absorption in the aggregate P3HT suggesting that the orientation of the P3HT plays a role in the device variation. The change in photoresponse is similar to previous results that considered the molecular orientation of zinc phthalocyanine (ZnPc) at a heterojunction with C_{60}.[6] In that work, quantum chemical calculations showed that the charge transfer dissociation efficiency for excitons generated in the ZnPC was shown to have a larger dependence on ZnPc orientation than excitons generated in the C_{60} acceptor.[6] A similar mechanism may exist in the P3HT/PCBM system; however, a large number of variables will influence the photogeneration of carriers, and the

DOI: 10.1021/am508855s
ACS Appl. Mater. Interfaces 2015, 7, 13208−13216

specific cause of the differences in short circuit current between PHJ cells remains a topic of future work.

3. CONCLUSION

In this study, P3HT/PCBM PHJ OPV cells were fabricated with variation in P3HT processing conditions. The variation in P3HT processing was shown to primarily modify the out-of-plane molecular orientation in the films, resulting in six unique P3HT orientation distributions as characterized by X-ray diffraction. The relative orientation of P3HT was then shown to have a significant impact on the open-circuit voltage (V_{OC}) of the OPV cells. This is attributed to the variation in ΔE_{HL} at the heterojunction due to a shift in HOMO energy level of the P3HT. The change in P3HT HOMO energy level is estimated using DFT modeling of the IE with molecular orientation. A linear relationship is found between V_{OC} and P3HT HOMO energy level when the energy level is defined by a compositional average of the crystalline P3HT out-of-plane stacking distribution. This result is supported by equivalent circuit modeling, where V_{OC} is shown to have a linear dependence on ΔE_{HL}. The alloy-like behavior with molecular orientation is believed to exist due to the extended wave function of the hole in the charge transfer state. These results have significant implications for future organic solar cell design where molecular orientation of polar molecules can be engineered to maximize not only charge transfer dissociation efficiency,[9,13] but also operating voltage.

4. EXPERIMENTAL METHODS

4.1. Film Preparation. The P3HT was obtained from Plextronics, Inc. with a number-averaged molecular mass M_n = 50 kDa, a regioregularity of 99%, and a polydispersity of 2.1.[39] The PCBM was obtained from Nano-C with a purity of 99%. The PEDOT:PSS solution was type PVP AI4083, obtained from Heraeus Materials Technology. PDMS was made from SYLGARD 184 Elastomer Kit from Dow Corning at a ratio of 15:1.[24] OTS was obtained from Gelest, Inc. The P3HT films were spun cast on octyltrichlorosilane (OTS) treated silicon at 500, 750, and 3,000 rpm from 3, 6, and 7 mg/mL chloroform solutions, and at 625, 850, and 3000 rpm from 6, 12, and 14 mg/mL 1,2-dichlorobenzene (DCB) solutions. The concentration of the P3HT solutions was varied to ensure a consistent final P3HT film thickness that ranged from 36 to 45 nm. Neat PCBM films were spun on silicon substrates at 2250 rpm from 35 mg/mL DCB solution resulting in a film thickness of approximately 38 nm. All substrates were cleaned by sonication for 10 min in deionized (DI) water, acetone, and isopropanol, followed by UV-ozone treatment for 10 min, and then rinsed with DI water. The OTS treatment followed a previously described procedure.[24] PEDOT:PSS films were spun on indium tin oxide (ITO) coated glass at 5000 rpm for 60 s and then annealed inside a glovebox at 120 °C for 20 min.

4.2. Device Construction. Planar heterojunction devices were constructed by transfer printing consecutive layers of P3HT and PCBM onto PEDOT:PSS and ITO coated glass substrates. The P3HT films were initially cast of OTS treated Si. A polydimethylsiloxane (PDMS) stamp is then laminated to the P3HT film and quickly removed resulting in complete transfer of the P3HT to the PDMS. The P3HT coated PDMS is then laminated to the PEDOT:PSS and ITO coated glass substrate and removed with a slight shear load resulting in P3HT transferring completely to the PEDOT:PSS surface. For biaxially strained P3HT films, the P3HT film is strained uniaxially while on the PDMS stamp by 100% strain and then transfer printed back onto a OTS treated silicon substrate. It is laminated back onto the same PDMS stamp and strained uniaxially by 100% in the transverse direction and then printed onto the PEDOT:PSS layer of the OPV cell. In the case of PCBM, the PCBM film was initially cast on a silicon substrate with a native oxide layer. The PDMS stamp was then laminated onto the PCBM and the stack was immersed in DI water resulting in delamination of the silicon substrate and complete transfer to the PDMS. The film was then thoroughly dried with nitrogen gas and laminated onto the P3HT layer. The PDMS is slowly removed by transferring the PCBM film onto the partially fabricated OPV cell. P3HT printing was performed in a N_2 filled glovebox while PCBM printing is performed in atmosphere. The printing process is the same method previously shown to result in a sharp interface.[19,20] This includes the demonstration of bilayers after metal deposition,[20] providing confidence that the electrode deposition in this study does not induce unintentional mixing.[20] The OPV cell was completed by depositing the cathode by vacuum thermal evaporation at a pressure of 1×10^{-6} Torr. The cathode consisted of ~1 nm lithium fluoride and ~100 nm aluminum film. The bulk heterojunction films were processed from 30 mg/mL solution at a 1:1 P3HT:PCBM ratio by mass in DCB solvent. The solution is spun cast at 600 rpm for 30 s and then placed in a covered Petri dish to dry slowly for 1 h. The films were then thermally annealed uncovered at 110 °C for 10 min.

4.3. Morphology Characterization. The thickness of the films was determined using a Woollam variable-angle spectroscopic ellipsometer (VASE). Absorbance measurements were made using an Ocean Optics Jazz spectrometer. Absorbance was measured for P3HT/PCBM bilayer films on PEDOT:PSS and ITO coated glass substrates. The reported absorbance was corrected by subtracting the absorbance of a PEDOT:PSS and ITO coated glass substrate. X-ray diffraction was performed at the Stanford Synchrotron Radiation Lightsource (SSRL) on beamline 11-3 with an area detector (MAR345 image plate), an energy of 12.735 keV, and an incidence angle of ≈0.12°. For the biaxially strained films, the sample was aligned with the X-ray beam parallel to the first and second strain directions. In these measurements, the sample chambers were purged with helium to reduce beam damage and background scattering. The pole figures are corrected for the fixed incident angle of the GIXD geometry and the $\sin(\omega)$ to account for the film geometry. The uncertainty in the calculated P3HT HOMO energy level is estimated by considering the variation in GIXD pole figures of the biaxially strained films. The film with the largest difference in predicted energy levels (DCB-X) was used to estimate uncertainty with the difference in estimated HOMO energy level taken as the confidence interval.

4.4. Electrical Characterization. The organic photovoltaic devices were tested using a Newport 150 W solar simulator with an AM1.5G filter under 1-sun (100 mW/cm^2) conditions, referenced to an NREL certified Si solar cell. The OPV device area is 3.14 mm^2, and the device performance is not corrected for spectral mismatch. The reported current−voltage characteristics are representative devices. The device performance in Table 2 is based on a minimum of 6 devices from multiple experiments except the fast cast chloroform film, which is based on 2 devices. The uncertainty is given as 1 standard deviation of the mean.

The external quantum efficiency was measured using light from a Newport 150 W solar simulator with an AM1.5G filter in combination with Newport 7400 Cornerstone 130 1/8m monochromator. The response was recorded as the current over a 1 MΩ resistance, using a Stanford Research Systems SR830 lock-in amplifier. A Newport 818-UV silicon low power photodetector was used as a reference.

■ ASSOCIATED CONTENT

Ⓢ Supporting Information

Additional figures and tables on H-aggregate model fits to absorbance data, X-ray pole figures, dark current $J-V$ curves, and resistance models. The Supporting Information is available free of charge on the ACS Publications website at DOI: 10.1021/am508855s.

■ AUTHOR INFORMATION

Corresponding Author

*E-mail: btoconno@ncsu.edu.

DOI: 10.1021/am508855s
ACS Appl. Mater. Interfaces 2015, 7, 13208−13216

Notes

The authors declare no competing financial interest.

■ ACKNOWLEDGMENTS

This research work was supported in part by the National Science Foundation (Award 1200340) and North Carolina Space Grant (Award 2011-1863). Portions of this research were carried out at the Stanford Synchrotron Radiation Lightsource, a Directorate of SLAC National Accelerator Laboratory and an Office of Science User Facility operated for the U.S. Department of Energy Office of Science by Stanford University. We thank Michael F. Toney for assistance with the X-ray diffraction measurements. AFM characterization by T.M. and H.A. and contributions to the manuscript were supported by DOE, OS, BES, Division of Materials Science and Engineering under Contract DE-FG02-98ER45737.

■ REFERENCES

(1) Deibel, C.; Dyakonov, V. Polymer-Fullerene Bulk Heterojunction Solar Cells. *Rep. Prog. Phys.* **2010**, *73*, 096401.

(2) Blom, P. W. M.; Mihailetchi, V. D.; Koster, L. J. A.; Markov, D. E. Device Physics of Polymer:Fullerene Bulk Heterojunction Solar Cells. *Adv. Mater.* **2007**, *19*, 1551−1566.

(3) Vandewal, K.; Tvingstedt, K.; Gadisa, A.; Inganas, O.; Manca, J. V. Relating the Open-Circuit Voltage to Interface Molecular Properties of Donor:Acceptor Bulk Heterojunction Solar Cells. *Phys. Rev. B* **2010**, *81*, 125204.

(4) Potscavage, W. J.; Sharma, A.; Kippelen, B. Critical Interfaces in Organic Solar Cells and Their Influence on the Open-Circuit Voltage. *Acc. Chem. Res.* **2009**, *42*, 1758−1767.

(5) Yi, Y.; Coropceanu, V.; Bredas, J. L. Exciton-Dissociation and Charge-Recombination Processes in Pentacene/C-60 Solar Cells: Theoretical Insight into the Impact of Interface Geometry. *J. Am. Chem. Soc.* **2009**, *131*, 15777−15783.

(6) Rand, B. P.; Cheyns, D.; Vasseur, K.; Giebink, N. C.; Mothy, S.; Yi, Y.; Coropceanu, V.; Beljonne, D.; Cornil, J.; Bredas, J.-L.; Genoe, J. The Impact of Molecular Orientation on the Photovoltaic Properties of a Phthalocyanine/Fullerene Heterojunction. *Adv. Funct. Mater.* **2012**, *22*, 2987−2995.

(7) Ratcliff, E. L.; Garcia, A.; Paniagua, S. A.; Cowan, S. R.; Giordano, A. J.; Ginley, D. S.; Marder, S. R.; Berry, J. J.; Olson, D. C. Investigating the Influence of Interfacial Contact Properties on Open Circuit Voltages in Organic Photovoltaic Performance: Work Function Versus Selectivity. *Adv. Energy Mater.* **2013**, *3*, 647−656.

(8) Rand, B. P.; Burk, D. P.; Forrest, S. R. Offset Energies at Organic Semiconductor Heterojunctions and their Influence on the Open-Circuit Voltage of Thin-Film Solar Cells. *Phys. Rev. B* **2007**, *75*, 115327.

(9) Ojala, A.; Petersen, A.; Fuchs, A.; Lovrincic, R.; Poelking, C.; Trollmann, J.; Hwang, J.; Lennartz, C.; Reichelt, H.; Hoeffken, H. W.; Pucci, A.; Erk, P.; Kirchartz, T.; Wuerthner, F. Merocyanine/C60 Planar Heterojunction Solar Cells: Effect of Dye Orientation on Exciton Dissociation and Solar Cell Performance. *Adv. Funct. Mater.* **2012**, *22*, 86−96.

(10) Park, Y. D.; Cho, J. H.; Kim, D. H.; Jang, Y.; Lee, H. S.; Ihm, K.; Kang, T. H.; Cho, K. Energy-level Alignment at Interfaces Between Gold and Poly(3-hexylthiophene) Films with Two Different Molecular Structures. *Electrochem. Solid-State. Lett.* **2006**, *9*, G317−G319.

(11) Tada, A.; Geng, Y.; Wei, Q.; Hashimoto, K.; Tajima, K. Tailoring Organic Heterojunction Interfaces in Bilayer Polymer Photovoltaic Devices. *Nat. Mater.* **2011**, *10*, 450−455.

(12) Chen, W.; Qi, D. C.; Huang, Y. L.; Huang, H.; Wang, Y. Z.; Chen, S.; Gao, X. Y.; Wee, A. T. S. Molecular Orientation Dependent Energy Level Alignment at Organic-Organic Heterojunction Interfaces. *J. Phys. Chem. C* **2009**, *113*, 12832−12839.

(13) Tumbleston, J. R.; Yang, L.; Collins, B. A.; Stuart, A. C.; Gan, E.; Ma, W.; You, W.; Ade, H. Molecular Orientation with Respect to Organic Bulk Heterojunctions Is a Key Factor for Solar Cell Performance. *Nat. Photonics* **2014**, *8*, 385−391.

(14) Heimel, G.; Salzmann, I.; Duhm, S.; Rabe, J. P.; Koch, N. Intrinsic Surface Dipoles Control the Energy Levels of Conjugated Polymers. *Adv. Funct. Mater.* **2009**, *19*, 3874−3879.

(15) Turner, S. T.; Pingel, P.; Steyrleuthner, R.; Crossland, E. J. W.; Ludwigs, S.; Neher, D. Quantitative Analysis of Bulk Heterojunction Films Using Linear Absorption Spectroscopy and Solar Cell Performance. *Adv. Funct. Mater.* **2011**, *21*, 4640−4652.

(16) Campoy-Quiles, M.; Ferenczi, T.; Agostinelli, T.; Etchegoin, P. G.; Kim, Y.; Anthopoulos, T. D.; Stavrinou, P. N.; Bradley, D. D. C.; Nelson, J. Morphology Evolution via Self-Organization and Lateral and Vertical Diffusion in Polymer:Fullerene Solar Cell Blends. *Nat. Mater.* **2008**, *7*, 158−164.

(17) Wang, D. H.; Choi, D. G.; Lee, K. J.; Im, S. H.; Park, O. O.; Park, J. H. Unexpected Solid-Solid Intermixing in a Bilayer of Poly(3-hexylthiophene) and [6,6]-Phenyl C61-Butyric Acid Methyl Ester Via Stamping Transfer. *Org. Electron.* **2010**, *11*, 1376−1380.

(18) Meitl, M. A.; Zhu, Z. T.; Kumar, V.; Lee, K. J.; Feng, X.; Huang, Y. Y.; Adesida, I.; Nuzzo, R. G.; Rogers, J. A. Transfer Printing by Kinetic Control of Adhesion to an Elastomeric Stamp. *Nat. Mater.* **2006**, *5*, 33−38.

(19) Ro, H. W.; Akgun, B.; O'Connor, B.; Hammond, M. R.; Kline, R. J.; Snyder, C. R.; Satija, S. K.; Ayzner, A. L.; Toney, M. F.; Soles, C. L.; DeLongchamp, D. M. Mixing Behavior between P3HT and PCBM. *Macromolecules* **2012**, *45*, 6587−6599.

(20) Herzing, A. A.; Ro, H. W.; Soles, C. L.; DeLongchamp, D. M. Visualization of Phase Evolution in Model Organic Photovoltaic Structures via Energy-Filtered Transmission Electron Microscopy. *ACS Nano* **2013**, *7*, 7937−7944.

(21) Treat, N. D.; Brady, M. A.; Smith, G.; Toney, M. F.; Kramer, E. J.; Hawker, C. J.; Chabinyc, M. L. Interdiffusion of PCBM and P3HT Reveals Miscibility in a Photovoltaically Active Blend. *Adv. Energy Mater.* **2011**, *1*, 82−89.

(22) DeLongchamp, D. M.; Vogel, B. M.; Jung, Y.; Gurau, M. C.; Richter, C. A.; Kirillov, O. A.; Obrzut, J.; Fischer, D. A.; Sambasivan, S.; Richter, L. J.; Lin, E. K. Variations in Semiconducting Polymer Microstructure and Hole Mobility with Spin-Coating Speed. *Chem. Mater.* **2005**, *17*, 5610−5612.

(23) O'Connor, B.; Kline, R. J.; Conrad, B. R.; Richter, L. J.; Gundlach, D.; Toney, M. F.; DeLongchamp, D. M. Anisotropic Structure and Charge Transport in Highly Strain-Aligned Regioregular Poly(3-hexylthiophene). *Adv. Funct. Mater.* **2011**, *21*, 3697−3705.

(24) Gargi, D.; Kline, R. J.; DeLongchamp, D. M.; Fischer, D. A.; Toney, M. F.; O'Connor, B. T. Charge Transport in Highly Face-On Poly(3-hexylthiophene) Films. *J. Phys. Chem. C* **2013**, *117*, 17421−17428.

(25) Kim, J. B.; Guan, Z. L.; Lee, S.; Pavlopoulou, E.; Toney, M. F.; Kahn, A.; Loo, Y. L. Modular Construction of P3HT/PCBM Planar-Heterojunction Solar Cells by Lamination Allows Elucidation of Processing-Structure-Function relationships. *Org. Electron.* **2011**, *12*, 1963−1972.

(26) Spano, F. C. Modeling disorder in polymer aggregates: The Optical Spectroscopy of Regioregular Poly(3-hexylthiophene) Thin Films. *J. Chem. Phys.* **2005**, *122*, 234701.

(27) Clark, J.; Chang, J. F.; Spano, F. C.; Friend, R. H.; Silva, C. Determining Exciton Bandwidth and Film Microstructure in Polythiophene Films Using Linear Absorption Spectroscopy. *Appl. Phys. Lett.* **2009**, *94*, 163306.

(28) Gierschner, J.; Huang, Y. S.; Van Averbeke, B.; Cornil, J.; Friend, R. H.; Beljonne, D. Excitonic Versus Electronic Couplings in Molecular Assemblies: The Importance of Non-Nearest Neighbor Interactions. *J. Chem. Phys.* **2009**, *130*, 044105.

(29) Ferenczi, T. A. M.; Nelson, J.; Belton, C.; Ballantyne, A. M.; Campoy-Quiles, M.; Braun, F. M.; Bradley, D. D. C. Planar Heterojunction Organic Photovoltaic Diodes via a Novel Stamp Transfer Process. *J. Phys.: Condens. Matter* **2008**, *20*, 475203.

(30) Perez, M. D.; Borek, C.; Forrest, S. R.; Thompson, M. E. Molecular and Morphological Influences on the Open Circuit Voltages

DOI: 10.1021/am508855s
ACS Appl. Mater. Interfaces 2015, 7, 13208−13216

of Organic Photovoltaic Devices. *J. Am. Chem. Soc.* **2009**, *131*, 9281−9286.
(31) Fahrenbruch, A. L.; Aronvich, J. Heterojunction Phenomena and Interfacial Defects in Photovoltaic Converters. *Solar Energy Conversion—Solid State Physics Aspects*; Springer-Verlag: Berlin, 1979; Vol. *31*, pp 257−326.
(32) Mihailetchi, V. D.; Koster, L. J. A.; Blom, P. W. M. Effect of Metal Electrodes on the Performance of Polymer:Fullerene Bulk Heterojunction Solar Cells. *Appl. Phys. Lett.* **2004**, *85*, 970−972.
(33) Goh, C.; Kline, R. J.; McGehee, M. D.; Kadnikova, E. N.; Frechet, J. M. J. Molecular-Weight-Dependent Mobilities in Regioregular Poly(3-hexyl-thiophene) Diodes. *Appl. Phys. Lett.* **2005**, *86*, 122110.
(34) DeLongchamp, D. M.; Kline, R. J.; Herzing, A. Nanoscale Structure Measurements for Polymer-Fullerene Photovoltaics. *Energy Environ. Sci.* **2012**, *5*, 5980−5993.
(35) Yamamoto, S.; Orimo, A.; Ohkita, H.; Benten, H.; Ito, S. Molecular Understanding of the Open-Circuit Voltage of Polymer:-Fullerene Solar Cells. *Adv. Energy Mater.* **2012**, *2*, 229−237.
(36) Graham, K. R.; Erwin, P.; Nordlund, D.; Vandewal, K.; Li, R.; Ndjawa, G. O. N.; Hoke, E. T.; Salleo, A.; Thompson, M. E.; McGehee, M. D.; Amassian, A. Re-Evaluating the Role of Sterics and Electronic Coupling in Determining the Open-Circuit Voltage of Organic Solar Cells. *Adv. Mater.* **2013**, *25*, 6076−6082.
(37) Street, R. A.; Davies, D.; Khlyabich, P. P.; Burkhart, B.; Thompson, B. C. Origin of the Tunable Open-Circuit Voltage in Ternary Blend Bulk Heterojunction Organic Solar Cells. *J. Am. Chem. Soc.* **2013**, *135*, 986−989.
(38) Koster, L. J. A.; Mihailetchi, V. D.; Ramaker, R.; Blom, P. W. M. Light Intensity Dependence of Open-Circuit Voltage of Polymer:-Fullerene Solar Cells. *Appl. Phys. Lett.* **2005**, *86*, 123509.
(39) Certain commercial equipment or materials are identified in this paper in order to specify the experimental procedure adequately. Such identification is not intended to imply recommendation or endorsement by the National Institute of Standards and Technology, nor is it intended to imply that the materials or equipment identified are necessarily the best available for the purpose.

DOI: 10.1021/am508855s
ACS Appl. Mater. Interfaces 2015, 7, 13208−13216